Berezinskii—Kosterlitz—Thouless correlations in copper-based quasi-2D spin systems

Opherden, D.; Bärtl, F.; Tepaske, M. S. J.; Landee, C. P.; Wosnitza, J.; Kühne, H.;

Originally published:

July 2023

Low Temperature Physics 49(2023), 819-826

DOI: https://doi.org/10.1063/10.0019692

Low Temperature Physics/Fizyka Nyzkykh Temperatur, 2023, Vol. 49, No. 7, pp. 899–907

Berezinskii–Kosterlitz–Thouless correlations in copper-based quasi-2D spin systems

D. Opherden[1], F. Bärtl[1,2], M. S. J. Tepaske[3], C. P. Landee[4], J. Wosnitza[1,2], and H. Kühne[1]

(Review Article)

[1]*Hochfeld-Magnetlabor Dresden (HLD-EMFL) and Würzburg-Dresden Cluster of Excellence ct.qmat, Helmholtz-Zentrum Dresden-Rossendorf, Dresden 01328, Germany*

[2]*Institut für Festkörper- und Materialphysik, TU Dresden, Dresden 01062, Germany*

[3]*Physikalisches Institut, Universität Bonn, Bonn 53115, Germany*

[4]*Department of Physics, Clark University, Worcester MA 01610, USA*

E-mail: h.kuehne@hzdr.de

Received March 21, 2023, published online May 26, 2023

We present an overview of selected copper-based quasi-2D square-lattice spin-1/2 materials with an easy-plane anisotropy, providing the possibility to study emergent Berezinskii–Kosterlitz–Thouless (BKT) correlations. In particular, in those materials with a comparatively small exchange coupling, the effective *XY* anisotropy of the low-temperature spin correlations can be controlled by an applied magnetic field, yielding a systematic evolution of the BKT correlations. In cases where the residual interlayer correlations are small enough, dynamical BKT correlations in the critical regime may be observed experimentally, whereas the completion of the genuine BKT transition is preempted by the onset of long-range order.

Keywords: spin-1/2 square lattice, easy-plane anisotropy, long-range order, BKT transition, Nuclear magnetic resonance, *XY* model, Heisenberg model.

1. Introduction

Due to its importance as a fundamental model system in quantum magnetism, the two-dimensional quantum Heisenberg spin-1/2 antiferromagnet (2DQHAF) on a square lattice and its ground-state properties, as well as the influence of small perturbations and magnetic fields on the spin correlations, were investigated in numerous works over the past decades. In the presence of an XY anisotropy, the occurrence of the topological Berezinskii–Kosterlitz–Thouless phase transition at a finite temperature T_{BKT} [1–3], which marks the binding of topological defects in vortex-antivortex pairs, is a phenomenon of particular interest. Whereas the BKT transition is often studied for the spin-1/2 case, it occurs also in the classical limit [4, 5]. In the reported experimental studies, the investigation of a genuine BKT transition in bulk materials was compromised by the onset of long-range order (LRO) [6–12]. Typically, a residual interlayer coupling J' stabilizes LRO at temperatures above T_{BKT}, thus preventing the manifestation of the BKT transition in material realizations of the 2D XY model. Still, if the perturbations relative to the 2D XY model are small enough, the spin system may yield experimental signatures of BKT-type correlations that develop at temperatures approaching T_{LRO} [12–19].

The 2D spin-1/2 Heisenberg square-lattice antiferromagnet with weak easy-plane anisotropy in an applied magnetic field can be described by the Hamiltonian

$$\mathcal{H} = J \sum_{\langle i,j \rangle_{\parallel}} \left[S_i^x S_j^x + S_i^y S_j^y + (1-\Delta) S_i^z S_j^z \right] + J' \sum_{\langle i,j \rangle_{\perp}} \mathbf{S}_i \cdot \mathbf{S}_j - g\mu_B \mu_0 H \sum_i S_i^z , \quad (1)$$

where $\langle i,j \rangle_{\parallel}$ and $\langle i,j \rangle_{\perp}$ denote the intra- and interlayer nearest neighbors, and J and J' are the intra- and interlayer exchange couplings, respectively. Whereas $\Delta = 0$ corresponds to the isotropic Heisenberg case, $0 < \Delta \leq 1$ denotes a nonzero XY anisotropy.

For a small exchange coupling J of a few K, the application of experimentally available magnetic fields of seve-

ral T offers the possibility to continuously tune the low-temperature spin correlations from the 2D Heisenberg to the 2D XY limit [12, 20–26]. As was shown by numerical and analytical calculations, a uniform magnetic field breaks the $O(3)$ symmetry of the 2D quantum Heisenberg antiferromagnet, but preserves the easy-plane $O(2)$ symmetry [21]. Correspondingly, for Zeeman energies of the order of the exchange energy, the resulting effective XY anisotropy can be controlled. The associated BKT transition persists for all fields below the saturation field, yielding a nonmonotonic magnetic phase diagram [21]. This provides an excellent possibility for experimental studies of BKT physics and their comparison to theoretical predictions.

2. Classification of quasi-2D materials

In contrast to an ideal 2D Heisenberg spin system, the magnetic layers in bulk materials yield a nonzero interlayer exchange J', and typically also a weak intrinsic anisotropy Δ_{int}, which is described by the anisotropy parameter Δ in Eq. (1). Thus, in order to characterize how well the spin system in a given material can be approximated by the 2D Heisenberg model, the parameters J' and Δ_{int} need to be determined. Nonzero values of J' and Δ_{int} lead to long-range order at a critical temperature T_{LRO}, in contrast to the ideal 2D spin-1/2 Heisenberg case, which does not reveal long-range order at finite temperatures [27]. Therefore, a first qualification of a material as a realization of the 2D spin-1/2 Heisenberg antiferromagnet may be defined by the ratio $k_B T_{LRO}/J$, which varies between zero and values approaching unity for the 2D and the 3D spin-1/2 Heisenberg cases, respectively [28].

In order to estimate the interlayer interaction J', an empirical form, proposed by Yasuda *et al*., is often used [29]:

$$k_B T_{LRO} = \frac{4\pi\rho_s}{2.43 - \ln(J'/J)}, \qquad (2)$$

where $\rho_s = 0.183J$ is the renormalized spin-stiffness. Since this estimate assumes $\Delta_{\text{int}} = 0$, it represents only an upper boundary of J' for weakly anisotropic materials. Both, the interlayer coupling J' as well as the easy-plane anisotropy Δ_{int}, may drive long-range order at nonzero temperatures. Therefore, the ratio J'/J, calculated for quasi-2DQHAFs with a finite Δ_{int} by means of Eq. (2), represents an upper limit of the interlayer coupling.

For a nonzero Δ_{int} and $J' = 0$, quantum Monte Carlo (QMC) calculations showed that, even for anisotropies as small as 10^{-3}, the critical behavior of the magnetic lattice resembles that of the Berezinskii–Kosterlitz–Thouless universality class. A weak logarithmic decrease of the T_{BKT} temperature with reduction of the spin anisotropy was determined as [30]

$$k_B T_{BKT} = \frac{4\pi\rho_s}{\ln(330/\Delta)}, \qquad (3)$$

with the spin stiffness $\rho_s = 0.177J$.

In Table 1, we present a list of several Cu-based materials and their experimentally determined parameters, i.e., the intralayer coupling J, the zero-field ordering temperature T_{LRO}, the ratio J'/J, the electronic g-factor, the anisotropy field H_A (corresponding to a spin-flop anomaly), the saturation field H_{sat}, and the estimated easy-plane anisotropy Δ_{int}.

Metal-organic materials, in which the magnetic Cu^{2+} ions are embedded into a matrix of organic molecules, represent a pathway for realizing a 2DQHAF on a square lattice with small exchange coupling J/k_B of several K. By an appropriate choice of molecular ligands and counterions, the syntheses of several such materials were reported [24, 31–39, 42]. Often, pyrazine (pz = $C_4H_4N_2$) molecules are used as ligands to link the Cu^{2+} ions in the magnetic quasi-2D layers. The canting of the pyrazine rings [43–45] and the choice of the counterions [46] determine the strength of the exchange interaction. For several Cu^{2+}-based molecular materials, a magnetic phase diagram in applied magnetic fields was reported [24, 31, 36, 47, 48]. Therein, the magnetic properties were mostly investigated by thermodynamic methods [24, 32, 36, 39, 42], thus missing local information about the magnetic correlations at low temperatures.

As mentioned above, a 2D square-lattice spin-1/2 system with XY anisotropy exhibits a topological transition at a finite temperature T_{BKT} [10, 30]. QMC results for the dependence of this BKT transition temperature on the anisotropy parameter Δ_{int} are presented as open symbols and solid or dashed lines in Fig. 1 [10, 30]. The black solid circles denote the experimentally obtained values of $k_B T_{LRO}/J$ versus Δ_{int} for selected quasi-2D weakly anisotropic QHAFs [34, 39, 50]. Where possible, Δ_{int} was determined by Eq. (5) from a characteristic minimum of the dc susceptibility at $T_{\text{min}} = T_{\text{co}}$, compare Table 1. For $Cu(pz)_2(ClO_4)_2$ and $Cu(pz)_2(BF_4)_2$, very similar values of Δ_{int} were found from measurements of the field- and temperature-dependent magnetization. For $[Cu(pz)_2(HF_2)](ClO_4)$, the experimentally determined value of $\Delta_{\text{int}} = H_A/H_{\text{sat}}$ was used. $[Cu(pz)_2(4\text{-phpy-O})_2](ClO_4)$ and $[Cu(pz)_2(pyO)_2](ClO_4)$ are very similar in their properties and composition. Hence, only the slightly better isolated second material is presented in Fig. 1. For $[Cu(pz)_2(HF_2)](PF_6)$ and $[Cu(pz)_2(pyO)_2](PF_6)_2$, an indirect estimate of Δ_{int} using ESR and specific-heat measurements from Refs. 24, 36 was used.

For the inorganic compound $Sr_2CuO_2Cl_2$, which is a well-known realization of the 2DQHAF model, the anisotropy parameter, evaluated from the spin-dispersion analysis [12, 51], is an order of magnitude larger than the estimate $\Delta_{\text{int}} = H_A/H_{\text{sat}} = 1.8\cdot10^{-4}$. However, the latter estimate of Δ_{int} suffers from the uncertainty of H_{sat}. From the dc-susceptibility minimum at $T_{\text{co}} \simeq 320$ K, reported in Ref. 50, $\Delta_{\text{int}} = 9.9\cdot10^{-4}$ was found by use of Eq. (5). Further, $Sr_2CuO_2Cl_2$ hosts extremely well-isolated magnetic layers, with a ratio $k_B T_{LRO}/J = 0.176$, from which

Table 1. Selected Cu^{2+}-based quasi-2D spin-1/2 Heisenberg square-lattice antiferromagnets [24, 32–41]. The exchange interaction J, the ordering temperature T_{LRO}, the g-factor (where available, both the in-plane and the out-of-plane components are listed), the anisotropy field H_A, as well as the saturation field H_{sat} are presented. The ratio J'/J of the inter- to intralayer coupling is estimated using Eq. (2). The anisotropy parameter Δ_{int} is calculated from the dc susceptibility minimum at T_{co} using Eq. (5). Indirect estimates of Δ_{int} from (*) ESR [36], (**) specific heat [24], (†) and renormalization of the spin-wave dispersion analysis [12] are shown as well.

	J/k_B, K	T_{LRO}, K	k_BT_{LRO}/J	J'/J	g-factor	H_A, T	H_{sat}, T	H_A/H_{sat}	Δ_{int}
$Cu(pz)_2(ClO_4)_2$	18.1	4.21	0.232	$5.6\cdot10^{-4}$	2.25 2.04	0.28	51.1	$5.5\cdot10^{-3}$	$4.6\cdot10^{-3}$
$Cu(pz)_2(BF_4)_2$	15.3	3.8	0.248	$1.1\cdot10^{-3}$	–	0.25	43	$5.8\cdot10^{-3}$	$6.2\cdot10^{-3}$
$Cu(pz)_2(ReO_4)_2$	15.1	4.2	0.278	$2.9\cdot10^{-3}$	2.13	–	42.7	–	–
$Cu(pz)_2(H_2O)_2Cr_2O_7$	4.7	< 1.6	< 0.34	$\lesssim 1.3\cdot10^{-2}$	2.13	–	13.3	–	–
$[Cu(pz)_2(NO_3)](PF_6)$	10.8	3.05	0.282	$3.3\cdot10^{-3}$	–	$7\cdot10^{-3}$	30	$2.3\cdot10^{-4}$	$1.2\cdot10^{-2}$
$[Cu(pz)_2(HF_2)](BF_4)$	6.3	1.54	0.244	$9.1\cdot10^{-4}$	2.13	–	18.0	–	–
$[Cu(pz)_2(HF_2)](ClO_4)$	7.2	1.91	0.265	$1.9\cdot10^{-3}$	2.26 2.07	0.08	20.2	$4\cdot10^{-3}$	–
$[Cu(pz)_2(HF_2)](PF_6)$	12.8	4.38	0.342	$1.4\cdot10^{-2}$	2.11	–	35.5	–	$3\cdot10^{-3}$ (*)
$[Cu(pz)_2(HF_2)](AsF_6)$	12.8	4.34	0.339	$1.3\cdot10^{-2}$	2.13	–	36.1	–	–
$[Cu(pz)_2(HF_2)](SbF_6)$	13.3	4.31	0.324	$9.4\cdot10^{-3}$	2.14	–	37.6	–	–
$[Cu(pz)_2(4\text{-phpy-}O)_2](ClO_4)$	7.5	1.63	0.217	$2.8\cdot10^{-4}$	2.26 2.04	0.11	21.1	$5.2\cdot10^{-3}$	–
$[Cu(pz)_2(pyO)_2](ClO_4)$	7.7	1.70	0.220	$3.3\cdot10^{-4}$	2.26 2.04	0.11	21.9	$5\cdot10^{-3}$	–
$[Cu(pz)_2(pyO)_2](PF_6)_2$	8.1	1.71	0.211	$2.1\cdot10^{-4}$	2.25 2.05	–	23.7	–	$7\cdot10^{-3}$ (**)
$[Cu(pz)_2(2\text{-HOpy})_2](PF_6)_2$ (≡ CuPOF)	**6.8**	**1.38(2)**	**0.203**	**$1.4\cdot10^{-4}$**	**2.29 2.07**	**0.36(4)**	**17.57 19.5**	**$1.85\cdot10^{-2}$**	**$0.9\cdot10^{-2}$**
$Sr_2CuO_2Cl_2$	≃ 1450	255	0.176	$2.4\cdot10^{-5}$	–	0.7	≃ 4000	$1.8\cdot10^{-4}$	$1.4\cdot10^{-3}$(†)
La_2CuO_4	≃ 1600	320	0.200	$1.2\cdot10^{-4}$	–	–	≃ 4500	–	$2\cdot10^{-4}$

$J'/J = 2.4\cdot10^{-5}$ can be estimated [13, 34, 49, 50]. However, the antiferromagnetic intralayer coupling of 1450 K yields extremely large saturation fields, which prohibits experimental studies of field-induced effects on the spin correlations.

In this context, the material $[Cu(pz)_2(2\text{-HOpy})_2](PF_6)_2$ (CuPOF in the following) is of particular interest. The values of J, T_{LRO}, J'/J, the g-factor, the saturation field H_{sat}, and the anisotropy field H_A, as well as the anisotropy parameter Δ_{int} were determined by various experimental probes [31, 52, 53]. When comparing CuPOF with the other materials listed in Table 1, it can be characterized as an excellent realization of a quasi-2DQHAF with a small nearest-neighbor interaction of $J/k_B = 6.8$ K.

3. Characteristic temperatures vs XY anisotropy

As shown in Fig. 1, for selected quasi-2D materials with a very weak interlayer interaction, such as $Sr_2CuO_2Cl_2$ and $[Cu(pz)_2(pyO)_2](PF6)_2$, the experimentally determined values of k_BT_{LRO}/J are very close to those of the QMC calculations of k_BT_{BKT}/J for a weakly anisotropic 2DQHAF. This indicates that the critical spin correlations of the BKT transition and those underlying the formation of long-range order are closely related in these materials. Following Refs. 12 and 30, a comparison of the experimentally observed spin-anisotropy crossover temperature T_{co} and the LRO transition temperature T_{LRO} with QMC calculations of T_{co} and T_{BKT} for a weakly anisotropic square-lattice 2DQHAF is presented in Fig. 2 for $Sr_2CuO_2Cl_2$ and CuPOF. For both materials, excellent agreement is observed for the characteristic temperatures T_{co}, T_{BKT}, and T_{LRO}. The larger value of $k_BT_{LRO}/J = 0.203$ for CuPOF, as compared to $k_BT_{LRO}/J = 0.176$ for $Sr_2CuO_2Cl_2$, is attributed only to the comparatively stronger intrinsic spin anisotropy in CuPOF. Therefore, the magnetic layers in CuPOF are concluded to be similarly well isolated as in $Sr_2CuO_2Cl_2$.

Due to the very weak coupling of the magnetic layers in CuPOF, with $J'/J \approx 1.4\cdot10^{-4}$ the small entropy change expected at the transition at T_{LRO} is beyond the experimental resolution of thermodynamic probes [31, 54]. On the other hand, μ^+SR is very sensitive to the local stag-

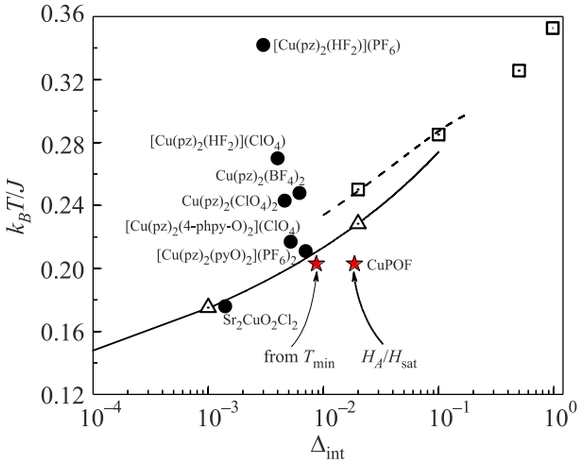

Fig. 1. Characteristic temperatures versus the anisotropy Δ_{int}. The open symbols denote QMC calculations of k_BT_{BKT}/J for weakly-anisotropic 2DQHAFs from [10] (open squares) and [30] (open triangles). Solid and dashed lines denote fits to the QMC data by empirical formulas from Refs. 30 and 10, respectively. Full circles denote k_BT_{LRO}/J of several quasi-2DQHAF materials with weak XY anisotropy Δ_{int} [34, 39, 50]. The full red stars represent k_BT_{LRO}/J of the material CuPOF versus estimates of the anisotropy parameter from the dc susceptibility and the anisotropy field, respectively [31].

gered magnetization, and was used to probe the transition to LRO at 1.38(2) K in CuPOF [31]. This transition occurs under the influence of the weak intrinsic easy-plane anisotropy, which yields a temperature-driven crossover from

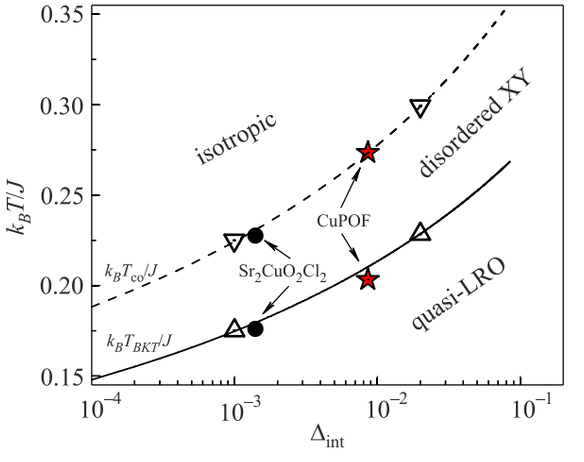

Fig. 2. Phase diagram for weakly anisotropic 2D spin-1/2 square-lattice Heisenberg antiferromagnets from Refs. 12, 30. The calculated BKT transition and spin-anisotropy crossover temperatures k_BT_{BKT}/J and k_BT_{co}/J, respectively, are presented as open up and down triangles. The temperatures k_BT_{co}/J and k_BT_{LRO}/J for $Sr_2CuO_2Cl_2$ and CuPOF are denoted by black circles and red stars, respectively. The dashed and solid lines are plots according to Eqs. (5) and (3), respectively.

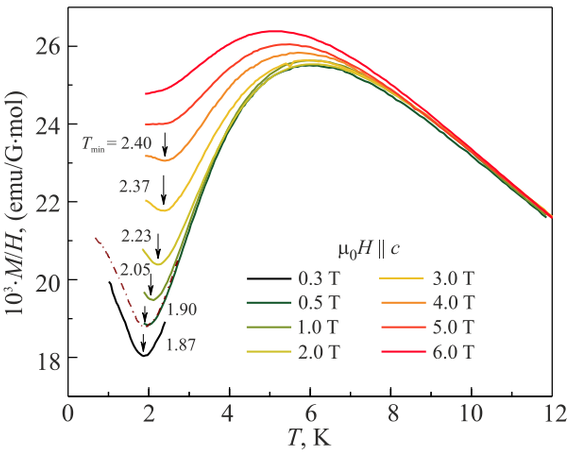

Fig. 3. (Color online) Molar dc susceptibility of single-crystalline CuPOF at different magnetic fields applied perpendicular to the crystallographic planes [31]. The black downward arrows indicate the crossover temperature, as discussed in the text.

isotropic to XY-type correlations at the crossover temperature $T_{\text{co}} > T_{LRO}$. An applied magnetic field increases the effective XY anisotropy, which manifests itself as a field-dependent minimum of the uniform bulk susceptibility at $T_{\text{min}} = T_{\text{co}}$, as depicted in Fig. 3.

4. XY anisotropy and characteristic temperatures vs field

A weak intrinsic anisotropy Δ_{int} can be determined from, e.g., measurements of the temperature- and field-dependent magnetization [12, 30, 34, 39, 50, 56]. A qualitatively different behavior of the field-dependent magnetization for magnetic fields applied parallel and perpendicular to the easy plane is expected at temperatures below T_{co}. At the anisotropy field H_A, a step-like feature of the in-plane magnetization occurs. Accordingly, H_A represents a measure of the spin-anisotropy and Δ_{int} can be evaluated as [57]:

$$\Delta_{\text{int}} = \frac{2Sg\mu_B H_A}{zJ} = \frac{H_A}{H_{\text{sat}}}, \qquad (4)$$

where $z = 4$ is the coordination number for a square lattice. For CuPOF, $H_A = 0.36(1)$ T, so that $\Delta_{\text{int}} = H_A / H_{\text{sat}} = 1.85(5)\cdot 10^{-2}$ is obtained as an estimate of the intrinsic easy-plane anisotropy [31]. The intrinsic anisotropy, caused by the combination of crystal electric field effects and residual spin-orbit coupling of the Cu^{2+} ions, is comparable for all metal-organic compounds in Table 1, resulting in similar values of the anisotropy fields H_A and components of the electronic g-factor.

As mentioned above, at fields above H_A, both the in- and out-of-plane dc susceptibility exhibit a broad minimum as a function of temperature. This anisotropic behavior can be understood in terms of the 2D Heisenberg model in the presence of a weak easy-plane anisotropy [12, 30, 34].

Cuccoli *et al*. reported an empirical formula for estimating the anisotropy parameter $\Delta_{\rm int}$ from the temperature of the minimum of the out-of-plane susceptibility at $T_{\rm min} = T_{\rm co}$ [12, 30]:

$$k_B T_{\rm co} = \frac{4\pi\rho_s}{\ln(160/\Delta)}, \qquad (5)$$

with the spin stiffness $\rho_s = 0.214J$. For CuPOF, employing Eq. (5) with $J/k_B = 6.8$ K and $T_{\rm co} = 1.86(5)$ K, we determine an anisotropy of $\Delta_{\rm int} = 0.9(2)\cdot 10^{-2}$.

In applied magnetic fields, a weakly-anisotropic quasi-2D Heisenberg spin system is described by the Hamiltonian (1). From analytical arguments [23, 58] and Monte Carlo simulations [20], it was established that, in the low-field regime, the 2DQHAF with $J' = \Delta_{\rm int} = 0$ in uniform magnetic fields exhibits an XY-like phase below $T_{\rm co}$. Thus, the isotropic 2DQHAF in applied magnetic fields can be mapped to a 2DQHAF with a weak easy-plane anisotropy by defining an effective field-induced anisotropy parameter Δ_{fi}. From comparing the QMC results of T_{BKT} for both these cases of the 2DQHAF, Cuccoli *et al*. [21] proposed a field-dependent anisotropy of the form $\Delta_{fi} \simeq h^2$ for the low-field regime, where $h = g\mu_B H/(JS)$ is the reduced magnetic field, with $h = 8$ at magnetic saturation. A comparison of the resulting characteristic temperatures is presented in Fig. 4. Here, the field-dependent temperatures $T_{\rm co}$ and T_{BKT} are presented as red stars and open circles, respectively. The black dashed line denotes the field dependence according to $t_{BKT}(h) \simeq (4\pi\rho_s/J)/\ln(C/h^2)$, where ρ_s is the spin stiffness and C a constant [21].

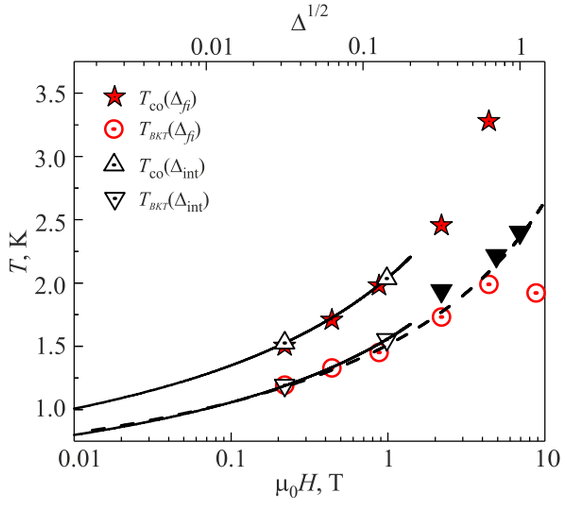

Fig. 4. (Color online) QMC results of $T_{\rm co}$ and T_{BKT} for a 2DQHAF with (i) a field-induced anisotropy Δ_{fi} and (ii) an intrinsic anisotropy $\Delta_{\rm int}$ [10, 12, 21, 30, 59]. Red stars and circles refer to the field-dependent temperatures $T_{\rm co}$ and T_{BKT} of the isotropic 2DQHAF [21]. Up and down triangles refer to $T_{\rm co}$ and T_{BKT} of the intrinsically anisotropic 2DQHAF from Ref. 30 (open symbols) and Refs. 10, 59 (solid symbols). The black solid lines denote the empirical expressions (5) and (3) for $T_{\rm co}$ and T_{BKT}, respectively, in the weakly-anisotropic regime [12, 30]. The magnetic field and the anisotropy parameter Δ are shown on the bottom and top horizontal scale, respectively. The temperatures and magnetic fields are scaled with the parameters of CuPOF, i.e., $J/k_B = 6.8$ K and $H_{{\rm sat},c} = 17.57(5)$ T.

Further, in Fig. 4, $T_{\rm co}$ and T_{BKT} for the weakly anisotropic 2DQHAF are plotted versus $\Delta^{1/2}$, since $\Delta_{fi} \simeq h^2$. Here, the solid down triangles are the QMC results from Refs. 10, 59, the open up and down triangles are the results from Ref. 30. In the low-field regime, a very good agreement between the QMC calculations for both cases of the 2DQHAF is found for both $T_{\rm co}$ and T_{BKT}. Thus, the effect of an increasing magnetic field applied to the isotropic 2DQHAF yields very similar spin correlations as an increase of the intrinsic easy-plane anisotropy in zero field.

An isotropic 2DQHAF in applied magnetic fields can be described by a renormalized planar rotator model with progressively decreasing rotator length [21]. By means of a detailed finite-size scaling analysis, Cuccoli *et al*. [21] verified an XY-type anisotropy of the spin system with a subsequent BKT transition for all magnetic fields up to the saturation field, regardless of the gradually reduced planar spin projection. Thus, the competing mechanisms of the field-induced XY anisotropy and the progressive spin canting in field direction govern the field-dependent evolution of T_{BKT}.

5. Field-driven evolution of the staggered magnetization

For a 2DQHAF in applied magnetic fields, upon cooling from the paramagnetic regime, Heisenberg-type spin correlations develop below $T \simeq J/k_B$, and cross over to a XY-type in the regime of $T_{\rm co}$. With further decreasing temperature, the spin correlation length ξ grows exponentially approaching the BKT transition at T_{BKT}. For $T \gtrsim T_{BKT}$, a rather low density of vortices is expected [60]. Furthermore, whereas Skyrmion-type textures may develop between about J/k_B and $T_{\rm co}$, the associated correlation length is rather short in this regime [53]. The exponential increase of ξ yields a rapid strengthening of the antiferromagnetic correlations in the XY regime and, therefore, the staggered magnetization becomes nonzero in a finite-size system. With further increase of ξ upon lowering the temperature, the magnetic correlations, due to the influence of the small but nonzero interlayer interaction J' on the regions with large in-plane correlation lengths, can no longer be treated as 2D. Therefore, a transition to long-range order occurs at T_{LRO}.

In order to investigate the effect of the field-tuned XY anisotropy on the static spin correlations in CuPOF, we probed the evolution of the staggered magnetization. The linewidth of the ^{31}P-NMR spectra, probing the local-field distribution at the ^{31}P sites, provides a measure of the staggered magnetization $m_{xy}(\pi,\pi,\pi)$. The temperature-dependent ^{31}P-NMR linewidth $\Delta\nu^{\star}$, recorded at 2 and 7 T, is presented in Fig. 5(a). The linewidth is normalized by the

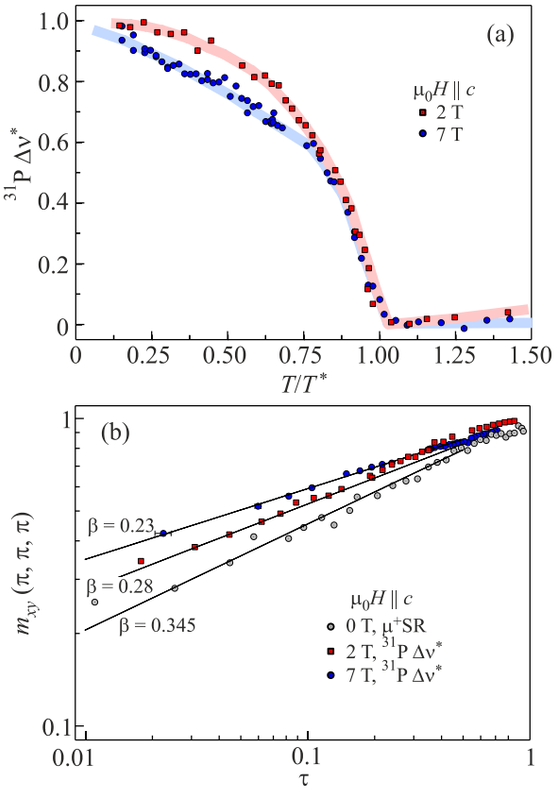

Fig. 5. (Color online) (a) Normalized ^{31}P-NMR linewidth $\Delta\nu^\star$, recorded at 2 and 7 T, plotted versus the reduced temperature $T/T^\star$. (b) Double-logarithmic plot of the staggered magnetization $m_{xy}(\pi,\pi,\pi)$, plotted versus the reduced temperature $\tau = (1 - T/T_c)$. At zero field, m_{xy} is probed by the normalized μ^+SR precession frequency. At 2 and 7 T, m_{xy} is probed by the normalized ^{31}P-NMR resonance linewidth $\Delta\nu^\star$. The black solid lines denote a power-law behavior according to $m_{xy} \propto \tau^\beta$.

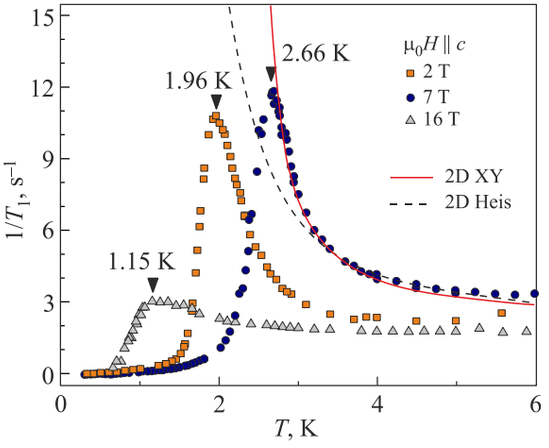

Fig. 6. (Color online) Temperature-dependent ^{31}P nuclear spin-lattice relaxation rate of CuPOF at 2, 7, and 16 T [53]. The downward triangles indicate the long-range ordering temperature T_{LRO}, determined as the rate maximum. For the data at 7 T, the dashed line indicates a fit with a 2D Heisenberg model between $T_{co} \approx 3.2$ K and $J/k_B = 6.8$ K. The red line indicates a fit with a 2D XY model between T_{LRO} and T_{co}.

low-temperature limit, $\Delta\nu \to 0$, as well as the x axis by the onset temperature $T^\star$ of a steeply increasing $\Delta\nu$. This onset occurs close to T_{LRO}, which is determined as the maximum of the temperature-dependent ^{31}P $1/T_1$ rate at given field, compare Fig. 6. In a 2D XY magnetic lattice, the correlation length increases exponentially as $\xi_{2DXY} \propto \exp(0.5\pi/\sqrt{T/T_{BKT} - 1})$ [2, 10]. In the presence of a finite interlayer coupling J', the transition to long-range order is expected at $\xi^2 J'/J \simeq 1$ [61]. With an in-plane correlation length of the order of 100 lattice spacings at T_{LRO} and $J'/J \simeq 1.4 \cdot 10^{-4}$ for CuPOF, the condition $\xi^2 J'/J \simeq 1$ is satisfied, and T_{LRO} may be interpreted as critical temperature T_c [53].

Closely below T_c, the staggered magnetization $m_{xy}(\pi,\pi,\pi)$ scales with the reduced temperature $\tau = (1 - T/T_c)$ as $m_{xy} \propto \tau^\beta$, where β may be interpreted as an effective critical exponent. Employing $T^\star \simeq T_c = 2.25$ K at 2 T and $T^\star \simeq T_c = 2.66$ K at 7 T, we plot the normalized ^{31}P linewidth as a function of the reduced temperature in a log-log plot, see Fig. 5(b). For the 7 T data, we find good agreement with the critical exponent $\beta_{2DXY} = 3\pi^2/128 \simeq 0.23$ of a finite-size 2D XY model [62, 63]. Similar observations were made for other materials that realize a planar XY lattice [17, 19, 64]. The same analysis was applied to data of the μ^+SR precession frequency at zero field [31], using $T_c = 1.38(2)$ K, giving $\beta = 0.345$, which is in good agreement with the theoretical critical exponent $\beta_{3D\text{Heis}} = 0.3639(35)$ [65] of the 3D Heisenberg model, and, similarly well, with the critical exponent $\beta_{3DXY} = 0.33$ [61] of the 3D XY model. At 2 T, we find $\beta = 0.28$, which may be interpreted in terms of a crossover between the Heisenberg and XY cases [66].

6. Field-driven evolution of the dynamic correlations

The temperature-dependent ^{31}P nuclear spin-lattice relaxation rate $1/T_1$ for out-of-plane magnetic fields of 2, 7, and 16 T is presented in Fig. 6. At high temperatures, $1/T_1$ is almost temperature-independent, indicating predominantly paramagnetic fluctuations. At temperatures above the onset of LRO, $1/T_1$ probes the dynamic correlation length ξ [15, 16, 67–70]. As was shown from dynamical scaling arguments [67], $1/T_1$ is proportional to the transverse spin correlation length as $1/T_1 \propto \xi^{z-\eta}$, where z and η are characteristic dynamic and critical exponents [15, 25, 67, 71]. In 2D magnetic lattices, the onset of short-range spin correlations occurs at temperatures $T \simeq J/k_B$ [54], with a correlation length of about one magnetic-lattice constant [10, 72]. To probe the crossover at T_{co}, we describe the ^{31}P $1/T_1$ rate

above $T_{co} \approx 3.2$ K with a 2D Heisenberg model, according to $\xi_{2D\text{Heis}} \propto \exp\left[2\pi 0.178 J/(k_B T)\right]$ [65, 72–75]. In contrast, we describe the data between T_{LRO} and T_{co} with a 2D XY model, according to $\xi_{2DXY} \propto \exp(0.5\pi/\sqrt{T/T_{BKT}-1})$ [2, 10]. Clearly, this comparison shows the formation of 2D XY correlations below T_{co} as a stronger increase of the temperature-dependent $1/T_1$ rate, compared to the increase according to the 2D Heisenberg model. A fit of $1/T_1$ in the interval $T_{LRO} \le T \le J/k_B$ with the 2D XY model yields T_{BKT} = 1.708(14), 2.237(7), and 0.90(16) K for applied fields of 2, 7, and 16 T, respectively, with errors determined by bootstrapping [53]. The BKT transition itself is preempted by the LRO that arises from the 3D correlations, stemming from the finite interlayer exchange interaction J'. At T_{LRO}, a sharp maximum of $1/T_1$ is observed for the two lower fields of 2 and 7 T. The amplitude of the $1/T_1$ maximum at 16 T, closely below the saturation field of 17.5 T, is substantially reduced in comparison.

With similar reasoning, for the case of $Sr_2CuO_2Cl_2$, it was argued that the LRO transition is induced by the incipient intralayer BKT transition at $T_{BKT} \lesssim T_{LRO}$ [10, 12]. Moreover, a spin-anisotropy crossover at $T_{co} \sim 320$ K was detected in measurements of the correlation length by means of neutron scattering [55] and NMR [14]. This is a very similar scenario of a spin-anisotropy crossover from isotropic Heisenberg correlations at $T > T_{co}$ to XY-like planar anisotropy at $T < T_{co}$ as we found for CuPOF.

7. Summary

We presented an overview and classification of several copper-based quasi-2D spin-1/2 square-lattice materials. These provide the opportunity to study Berezinskii–Kosterlitz–Thouless correlations, which emerge from a nonzero XY anisotropy. If the residual interlayer correlations are small enough, dynamic BKT correlations may be probed in the transition regime, whereas the completion of the genuine BKT transition is preempted by the onset of long-range order.

In particular, we discussed the material CuPOF as a model case for a 2DQHAF with small exchange coupling J, for which the application of a magnetic field allows a controlled tuning of the spin correlations from the almost isotropic 2D Heisenberg to the highly-anisotropic 2D XY limit. As a consequence of the field-induced BKT-type spin correlations, a concomitant nonmonotonic behavior of the transition temperature T_{LRO} is observed. The phenomenology in CuPOF is driven by field-induced Berezinskii–Kosterlitz–Thouless physics under the influence of extremely small interplane interactions, thus providing an opportunity for systematic investigations of BKT-type topological excitations.

Acknowledgments

We acknowledge the support of HLD at HZDR, member of the European Magnetic Field Laboratory (EMFL). This work was supported by the Deutsche Forschungsgemeinschaft (DFG) through SFB 1143 (project ID 247310070), the Würzburg-Dresden Cluster of Excellence on Complexity and Topology in Quantum Matter – *ct.qmat* (EXC 2147, project ID 390858490), and the cluster of excellence ML4Q (EXC 2004, project ID 390534769).

1. J. M. Kosterlitz and D. J. Thouless, *J. Phys. C* **6**, 1181 (1973).
2. J. M. Kosterlitz, *J. Phys. C* **7**, 1046 (1974).
3. V. L. Berezinskii, *J. Exp. Theor. Phys*. **32**, 493 (1971).
4. S. B. Khokhlachev, *Zh. Exp. Teor. Fiz*. **70**, 265 (1976).
5. L. Capriotti, A. Cuccoli, V. Tognetti, R. Vaia, and P. Verrucchi, *Physica D* **119**, 68 (1998).
6. B.-G. Liu, *Phys. Rev. B* **41**, 9563 (1990).
7. N. Majlis, S. Selzer, and G. C. Strinati, *Phys. Rev. B* **45**, 7872 (1992).
8. N. Majlis, S. Selzer, and G. C. Strinati, *Phys. Rev. B* **48**, 957 (1993).
9. L. Siurakshina, D. Ihle, and R. Hayn, *Phys. Rev. B* **61**, 14601 (2000).
10. H.-Q. Ding, *Phys. Rev. Lett*. **68**, 1927 (1992).
11. H.-Q. Ding, *J. Phys.: Condens. Matter* **2**, 7979 (1990).
12. A. Cuccoli, T. Roscilde, R. Vaia, and P. Verrucchi, *Phys. Rev. Lett*. **90**, 167205 (2003).
13. M. Greven, R. J. Birgeneau, Y. Endoh, M. A. Kastner, B. Keimer, M. Matsuda, G. Shirane, and T. R. Thurston, *Phys. Rev. Lett*. **72**, 1096 (1994).
14. B. J. Suh, F. Borsa, L. L. Miller, D. C. Johnston, D. R. Torgeson, and M. Corti, *J. Appl. Phys*. **79**, 5084 (1996).
15. B. J. Suh, F. Borsa, L. L. Miller, M. Corti, D. C. Johnston, and D. R. Torgeson, *Phys. Rev. Lett*. **75**, 2212 (1995).
16. D. Waibel, G. Fischer, T. Wolf, H. v. Löhneysen, and B. Pilawa, *Phys. Rev. B* **91**, 214412 (2015).
17. E. S. Klyushina, J. Reuther, L. Weber, A. T. M. N. Islam, J. S. Lord, B. Klemke, M. Månsson, S. Wessel, and B. Lake, *Phys. Rev. B* **104**, 064402 (2021).
18. N. Caci, L. Weber, and S. Wessel, *Phys. Rev. B* **104**, 155139 (2021).
19. P. Carretta, M. Filibian, R. Nath, C. Geibel, and P. J. C. King, *Phys. Rev. B* **79**, 224432 (2009).
20. D. P. Landau and K. Binder, *Phys. Rev. B* **24**, 1391 (1981).
21. A. Cuccoli, T. Roscilde, R. Vaia, and P. Verrucchi, *Phys. Rev. B* **68**, 060402(R) (2003).
22. W. J. M. de Jonge, J. P. A. M. Hijmans, F. Boersma, J. C. Schouten, and K. Kopinga, *Phys. Rev. B* **17**, 2922 (1978).
23. L. J. de Jongh and H. J. M. de Groot, *Solid State Commun*. **53**, 731 (1985).
24. Y. Kohama, M. Jaime, O. E. Ayala-Valenzuela, R. D. McDonald, E. D. Mun, J. F. Corbey, and J. L. Manson, *Phys. Rev. B* **84**, 184402 (2011).

25. *Magnetic Properties of Layered Transition Metal Compounds,* L. J. de Jongh (ed.), Springer, Netherlands (1990).
26. A. Iaizzi, H. D. Scammell, O. P. Sushkov, and A. W. Sandvik, *Phys. Rev. B* **101**, 104412 (2020).
27. N. D. Mermin and H. Wagner, *Phys. Rev. Lett.* **17**, 1133 (1966).
28. A. W. Sandvik, *Phys. Rev. Lett.* **80**, 5196 (1998).
29. C. Yasuda, S. Todo, K. Hukushima, F. Alet, M. Keller, M. Troyer, and H. Takayama, *Phys. Rev. Lett.* **94**, 217201 (2005).
30. A. Cuccoli, T. Roscilde, V. Tognetti, R. Vaia, and P. Verrucchi, *Phys. Rev. B* **67**, 104414 (2003).
31. D. Opherden, N. Nizar, K. Richardson, J. C. Monroe, M. M. Turnbull, M. Polson, S. Vela, W. J. A. Blackmore, P. A. Goddard, J. Singleton, E. S. Choi, F. Xiao, R. C. Williams, T. Lancaster, F. L. Pratt, S. J. Blundell, Y. Skourski, M. Uhlarz, A. N. Ponomaryov, S. A. Zvyagin, J. Wosnitza, M. Baenitz, I. Heinmaa, R. Stern, H. Kühne, and C. P. Landee, *Phys. Rev. B* **102**, 064431 (2020).
32. F. M. Woodward, P. J. Gibson, G. B. Jameson, C. P. Landee, M. M. Turnbull, and R. D. Willett, *Inorg. Chem.* **46**, 4256 (2007).
33. P. A. Goddard, J. Singleton, P. Sengupta, R. D. McDonald, T. Lancaster, S. J. Blundell, F. L. Pratt, S. Cox, N. Harrison, J. L. Manson, H. I. Southerland, and J. A. Schlueter, *New J. Phys.* **10**, 083025 (2008).
34. F. Xiao, F. M. Woodward, C. P. Landee, M. M. Turnbull, C. Mielke, N. Harrison, T. Lancaster, S. J. Blundell, P. J. Baker, P. Babkevich, and F. L. Pratt, *Phys. Rev. B* **79**, 134412 (2009).
35. J. L. Manson, K. H. Stone, H. I. Southerland, T. Lancaster, A. J. Steele, S. J. Blundell, F. L. Pratt, P. J. Baker, R. D. McDonald, P. Sengupta, J. Singleton, P. A. Goddard, C. Lee, M.-H. Whangbo, M. M. Warter, C. H. Mielke, and P. W. Stephens, *J. Am. Chem. Soc.* **131**, 4590 (2009).
36. E. Čižmár, S. A. Zvyagin, R. Beyer, M. Uhlarz, M. Ozerov, Y. Skourski, J. L. Manson, J. A. Schlueter, and J. Wosnitza, *Phys. Rev. B* **81**, 064422 (2010).
37. A. J. Steele, T. Lancaster, S. J. Blundell, P. J. Baker, F. L. Pratt, C. Baines, M. M. Conner, H. I. Southerland, J. L. Manson, and J. A. Schlueter, *Phys. Rev. B* **84**, 064412 (2011).
38. P. A. Goddard, J. L. Manson, J. Singleton, I. Franke, T. Lancaster, A. J. Steele, S. J. Blundell, C. Baines, F. L. Pratt, R. D. McDonald, O. E. Ayala-Valenzuela, J. F. Corbey, H. I. Southerland, P. Sengupta, and J. A. Schlueter, *Phys. Rev. Lett.* **108**, 077208 (2012).
39. P. A. Goddard, J. Singleton, I. Franke, J. S. Möller, T. Lancaster, A. J. Steele, C. V. Topping, S. J. Blundell, F. L. Pratt, C. Baines, J. Bendix, R. D. McDonald, J. Brambleby, M. R. Lees, S. H. Lapidus, P. W. Stephens, B. W. Twamley, M. M. Conner, K. Funk, J. F. Corbey, H. E. Tran, J. A. Schlueter, and J. L. Manson, *Phys. Rev. B* **93**, 094430 (2016).
40. T. Thio, T. R. Thurston, N. W. Preyer, P. J. Picone, M. A. Kastner, H. P. Jenssen, D. R. Gabbe, C. Y. Chen, R. J. Birgeneau, and A. Aharony, *Phys. Rev. B* **38**, 905 (1988).
41. N. S. Headings, S. M. Hayden, R. Coldea, and T. G. Perring, *Phys. Rev. Lett.* **105**, 247001 (2010).
42. V. Selmani, C. P. Landee, M. M. Turnbull, J. L. Wikaira, and F. Xiao, *Inorg. Chem. Commun.* **13**, 1399 (2010).
43. M. S. Haddad, D. N. Hendrickson, J. P. Cannady, R. S. Drago, and D. S. Bieksza, *J. Am. Chem. Soc.* **101**, 898 (1979).
44. H. W. Richardson, J. R. Wasson, and W. E. Hatfield, *Inorg. Chem.* **16**, 484 (1977).
45. J. Darriet, M. S. Haddad, E. N. Duesler, and D. N. Hendrickson, *Inorg. Chem.* **18**, 2679 (1979).
46. S. Vela, J. Jornet-Somoza, M. M. Turnbull, R. Feyerherm, J. J. Novoa, and M. Deumal, *Inorg. Chem.* **52**, 12923 (2013).
47. P. Sengupta, C. D. Batista, R. D. McDonald, S. Cox, J. Singleton, L. Huang, T. P. Papageorgiou, O. Ignatchik, T. Herrmannsdörfer, J. L. Manson, J. A. Schlueter, K. A. Funk, and J. Wosnitza, *Phys. Rev. B* **79**, 060409(R) (2009).
48. N. A. Fortune, S. T. Hannahs, C. P. Landee, M. M. Turnbull, and F. Xiao, *J. Phys. Conf. Ser.* **568**, 042004 (2014).
49. M. Greven, R. J. Birgeneau, Y. Endoh, M. A. Kastner, B. Keimer, M. Matsuda, G. Shirane, and T. R. Thurston, *Physica B* **199**, 642 (1994).
50. D. Vaknin, S. K. Sinha, C. Stassis, L. L. Miller, and D. C. Johnston, *Phys. Rev. B* **41**, 1926 (1990)
51. J. Igarashi, *J. Phys.: Condens. Matter* **4**, 10265 (1992).
52. D. Opherden, F. Bärtl, S. Yamamoto, Z. T. Zhang, S. Luther, S. Molatta, J. Wosnitza, M. Baenitz, I. Heinmaa, R. Stern, C. P. Landee, and H. Kühne, *Phys. Rev. B* **103**, 014428 (2021).
53. D. Opherden, M. S. J. Tepaske, F. Bärtl, M. Weber, M. M. Turnbull, T. Lancaster, S. J. Blundell, M. Baenitz, J. Wosnitza, C. P. Landee, R. Moessner, D. J. Luitz, and H. Kühne, *Phys. Rev. Lett.* **130**, 086704 (2023).
54. P. Sengupta, A. W. Sandvik, and R. R. P. Singh, *Phys. Rev. B* **68**, 094423 (2003).
55. D. Vaknin, L. L. Miller, J. L. Zarestky, and D. C. Johnston, *Physica C* **274**, 331 (1997).
56. M. Matsuura, K. Gilijamse, J. E. W. Sterkenburg, and D. J. Breed, *Phys. Lett. A* **33**, 363 (1970).
57. M. E. Lines, *J. Appl. Phys.* **40**, 1352 (1969).
58. Y. Okwamoto, *J. Phys. Soc. Jpn.* **53**, 2434 (1984).
59. H.-Q. Ding and M. S. Makivić, *Phys. Rev. B* **42**, 6827 (1990).
60. K. Yosida, *Theory of Magnetism,* Springer-Verlag, Berlin, Heidelberg (1996).
61. J. Als-Nielsen, S. T. Bramwell, M. T. Hutchings, G. J. McIntyre, and D. Visser, *J. Phys.: Condens. Matter* **5**, 7871 (1993).
62. S. T. Bramwell and P. C. W. Holdsworth, *J. Phys.: Condens. Matter* **5**, L53 (1993).
63. S. T. Bramwell and P. C. W. Holdsworth, *Phys. Rev. B* **49**, 8811 (1994).
64. A. Taroni, S. T. Bramwell, and P. C. W. Holdsworth, *J. Phys.: Condens. Matter* **20**, 275233 (2008).
65. M. Troyer, M. Imada, and K. Ueda, *J. Phys. Soc. Jpn.* **66**, 2957 (1997).
66. S. V. Isakov and R. Moessner, *Phys. Rev. B* **68**, 104409 (2003).

67. F. Borsa, M. Corti, T. Goto, A. Rigamonti, D. C. Johnston, and F. C. Chou, *Phys. Rev. B* **45**, 5756 (1992).
68. F. Tabak, A. Lascialfari, and A. Rigamonti, *J. Phys.: Condens. Matter* **5**, B31 (1993).
69. L. Bossoni, P. Carretta, R. Nath, M. Moscardini, M. Baenitz, and C. Geibel, *Phys. Rev. B* **83**, 014412 (2011).
70. P. Gaveau, J. P. Boucher, L. P. Regnault, and Y. Henry, *J. Appl. Phys*. **69**, 6228 (1991).
71. P. C. Hohenberg and B. I. Halperin, *Rev. Mod. Phys*. **49**, 435 (1977).
72. H.-Q. Ding and M. S. Makivić, *Phys. Rev. Lett*. **64**, 1449 (1990).
73. J.-K. Kim and M. Troyer, *Phys. Rev. Lett.* **80**, 2705 (1998).
74. M. Troyer, *Universality in Two-Dimensional Quantum Heisenberg Antiferromagnets*, in: *Open Problems in Strongly Correlated Electron Systems*, J. Bonča, P. Prelovšek, A. Ramšak, and S. Sarkar (eds.), *NATO Science Series*, Springer, Dordrecht (2001), Vol. 15.
75. P. Hasenfratz and F. Niedermayer, *Phys. Lett. B* **268**, 231 (1991).

Кореляції Березинського–Костерліца–Таулесса в квазі-2D спінових системах на основі міді (Огляд)

D. Opherden, F. Bärtl, M. S. J. Tepaske, C. P. Landee, J. Wosnitza, H. Kühne

Представлено огляд відібраних квазі-2D матеріалів із квадратною ґраткою зі спіном 1/2 на основі міді та легкоплощинною анізотропією, що дає можливість вивчати виникнення кореляцій Березинського–Костерліца–Таулесса (БКТ). Зокрема, у таких матеріалах із порівняно невеликим обмінним зв'язком ефективна *XY* анізотропія низькотемпературних спінових кореляцій може контролюватися прикладенням магнітного поля, що призводить до систематичної еволюції кореляцій БКТ. У випадках, коли залишкові міжшарові кореляції є досить малими, динамічні кореляції БКТ у критичному режимі можна спостерігати експериментально, тоді як завершення справжнього переходу БКТ попереджається виникненням дальнього порядку.

Ключові слова: спін-1/2 квадратна ґратка, легкоплощинна анізотропія, дальній порядок, БКТ перехід, ядерний магнітний резонанс, *XY* модель, модель Гейзенберга.